scientific reports

Check for updates

OPEN

Dual-energy CT-derived virtual noncalcium imaging to assess bone marrow lesions in patients with knee osteoarthritis

Wei Chen[1,5], Limin Liu[2,5], Heng Zhao[1,5], Hui Li[1,4], Jing Luo[1], Yao-lin Qu[1], Dan Zhang[1], Ya-han He[1], Yi-sha Pan[1], Fang Gao[1], Hua-zhi Liao[1], Xiao-long Chen[1], Hao Lei[1], De-qiu Tang[1] & Fei Peng[1,3]✉

To determine the diagnostic performance of dual-energy CT (DECT) virtual noncalcium (VNCa) technique in the detection of bone marrow lesions (BMLs) in knee osteoarthritis, and further analyze the correlation between the severity of BMLs on VNCa image and the degree of knee pain. 23 consecutive patients with clinically diagnosed knee osteoarthritis were underwent DECT and 3.0T MRI between August 2017 and November 2018. Evaluation of two pain assessment scales (WOMAC and KOOS) were collected. VNCa images and MRI were independently scored by three readers using a four-level scoring system over 15 anatomical subregions in each knee joint. Spearman correlation coefficient was used for total BML scores on DECT and MRI correlation with WOMAC and KOOS. Specificity, Sensitivity, NPV and PPV of reader 1 and reader 2 were 99.4%/99.2%, 89.4%/87.2%, 98.6%/98.3% and 95.5%/93.2%. A cutoff value of – 41.5 HU/– 46.5 HU provided sensitivities of 93.2%/90.9% and specificities of 100.0%/93.9% for diagnosing BMLs with AUC of 0.970/0.996. A stronger correlation was observed between the WOMAC and total BML score compared to the KOOS. DECT possessed excellent diagnostic performance in the detection of BMLs in knee osteoarthritis. And the pain degree increased with the severity of BMLs on VNCa images.

Keywords Bone marrow lesion, Pain, Knee osteoarthritis, Dual-energy CT, Virtual noncalcium

Abbreviations

BML	Bone marrow lesion
CI	Confidence interval
CRP	C-reactive protein
DECT	Dual-energy computed tomography
ESR	Erythrocyte sedimentation rate
KOOS	The Knee Injury and Osteoarthritis Outcome Score
OA	Osteoarthritis
SD	Standard deviation
VNCa	Virtual non-calcium
WOMAC	The Western Ontario and McMaster Universities Osteoarthritis Index

Osteoarthritis (OA) is a serious global health burden, with no effective treatment currently available, and is a major cause of functional impairment and disability in the elderly[1]. Common clinical symptoms of knee OA include knee pain, stiffness and swelling. Pain seriously affects the life quality and become the most common reason for patients to seek medical care.

[1]Department of Radiology, The First Affiliated Hospital, Hengyang Medical School, University of South China, Chuanshan Road No. 69, Hengyang 421001, Hunan, China. [2]Department of Ultrasound, The Second Affiliated Hospital, Hengyang Medical School, University of South China, Jiefang Road No. 35, Hengyang 421001, Hunan, China. [3]Department of Medical Imaging center, The Second Affiliated Hospital of Nanchang University, Minde Road No. 1, Nanchang 330006, Jiangxi, China. [4]Department of Radiology, The First People's Hospital of Zhaoqing, DonggangEast Road No.9, Zhaoqing 526060, Guangdong, China. [5]Wei Chen, Limin Liu and Heng Zhao contributed equally to this work. ✉email: pf520llm@163.com

Knee OA pain associates with various structural factors, such as knee effusion, synovial thickening/synovitis, bone marrow lesions (BMLs), and periarticular lesions (e.g. infrapatellar fat pad), etc[2,3]. Among these factors, BMLs are considered a relatively recent discovery[4], especially the subchondral BMLs, which are richly innervated with nociceptive pain fibers and may be a source of pain in patients with symptomatic degenerative joint disease[5–7]. The size of BMLs, what is resulted to the degree of pain in knee OA patients, have been shown by several studies[8–10]. Therefore, early and accurate identification of subchondral BMLs is of much significance for the early clinical intervention of pain in knee OA patients.

MRI is the optimum imaging method to depict BMLs[4,11]. However, the clinical application of MRI sometimes may be limited by contraindications or time-consuming. Dual-energy CT (DECT) has the ability to identify substances, and can create VNCa images by removing calcium from CT data, based on three-material decomposition model to describe BMLs[12,13], thus allowing the detection of BML in traumatic[11,14–18] and non-traumatic setting[12,19–26]. Specifically, DECT VNCa has good diagnostic performance in diagnosing non-traumatic BMLs in the ankle[24] foot[25], wrist[26] and hip joints[23]. Since non-enhanced conventional CT has certain deficiencies in the detection of pain related BMLs prior to the advent of DECT, as it is impeded by the overlying trabecular bone[11,19]. Encouragingly, the introduction of VNCa technique allows a new approach to show bone marrow, and offers the possibility to solve this issue.

We hypothesized that VNCa allows for both qualitative and quantitative analysis of OA-BML, and the severity of BMLs is correlated with the degree of pain. Therefore, this study aims to determine the diagnostic capability assessment of VNCa technique in detecting BMLs in knee OA, and further analyze the correlation between the severity of BMLs on VNCa and knee pain degree.

Materials and methods

This study was approved by the Institutional Review Board. It was also registered in China Clinical Trial Registry Center (Registration number: ChiCTR1900024305). All participants signed informed consent before examination. And all methods were performed in accordance with the relevant guidelines and regulations.

Study population

We retrospectively included 31 consecutive patients clinical diagnosed with knee osteoarthritis from August 2017 to November 2018, who underwent non-contrast DECT and 3.0T MRI examinations. DECT and MRI examinations were conducted within 24 h. Patients who subsequently diagnosed with bone tumor-like lesions ($n=2$), rheumatoid arthritis ($n=3$), bone infarction ($n=1$), and images of substandard quality ($n=2$) of the knee joint were excluded. Finally, 23 patients were included (Fig. 1), of which 19 patients had OA in unilateral knee joint and 4 patients had OA in bilateral knee joints (total 27 knee joints).

The establishment of clinical osteoarthritis diagnostic criteria based on the modified American College of Rheumatology, including the following points: recurrent episodes of knee arthralgia lasting for one month, asymmetric joint space narrowing, cystic degeneration and/or subchondral bone sclerosis, and osteophytes. Additionally, the synovial fluid should be clear and viscous on at least two times, with leukocyte counts below 2000/-mL. The duration of morning stiffness less than 30 min, and bony crepitus occurring during joint activity. Finally, normal or slightly elevated erythrocyte sedimentation rate (ESR) or C-reactive protein (CRP) levels[27–29]. The inclusion criteria for the study were as follows: Adhering to the modified American College of Rheumatology clinical diagnostic criteria for osteoarthritis as previously stated, the patient underwent relevant imaging examinations and agreed to sign an informed consent form.

The exclusion criteria included a patient age below 40 years, previous diagnosis of axial spondyloarthritis, rheumatoid arthritis, reactive arthritis, psoriatic arthritis, or any other type of chronic immune disease. Patients undergoing systemic corticosteroid therapy was also excluded, as well as those with contraindications to MRI. Lastly, any individuals who refused or were unable to participate (e.g. pregnant women) were also excluded[30–32].

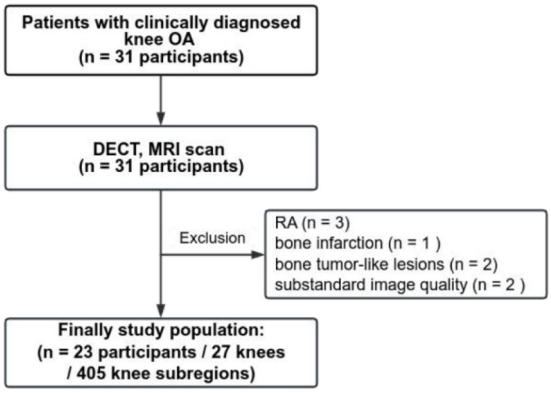

Fig. 1. The flowchart showed selection of study participants. *OA* = osteoarthritis, *DECT* = dual-energy computed tomography, *MRI* = magnetic resonance imaging, *RA* rheumatoid arthritis.

Clinical data and pain scale assessment

General data of the patients, such as age, gender, and history of trauma, etc. were collected. The Knee Injury and Osteoarthritis Outcome Score (KOOS) and The Western Ontario and McMaster Universities Osteoarthritis Index (WOMAC) were used to evaluate the pain of unilateral knee joint. The WOMAC (ranges from 0 to 96) covers 24 items of three aspects: function (17 items), pain (5 items), and stiffness (2 items)[33]. A lower WOMAC score indicates a lower level of symptoms or disability. KOOS covers quality of life (4 items), sport and recreation function (5 items), symptoms (7 items), pain (9 items), activities of daily living (17 items), scores range from 0 to 4 for each item. Afterwards, the scores were converted into a 0–100 scale. The higher the score in KOOS, the more serious the knee problem is[34].

DECT image acquisition

Knee joint in participants, qualitative and quantitative analysis using a DECT scanner (Somatom Definition Flash; Siemens Healthineers). This scanner is equipped with low (tube A, 80kVp) and high (tube B, 140kVp) kilovoltage X-ray tubes. CT scan of the knee was performed using a dual-energy pattern. The parameter settings for this pattern were: pitch of 0.7, collimation of 40 × 0.6 mm, and the rotation time of 1 s. All knees were placed in the supine position, feet first. The preset ratio of tube current-time product was 2:1 (tube A = 360mAs; tube B = 180 mAs) (Table S1). The mean volume CT dose index of this protocol, according to our study participant protocol, was 9.8 mGy ± 1.7 (standard deviation) (range, 8.2–15.3 mGy), and the mean dose-length product was 237.2 mGy cm ± 72.6 (range, 131.5–368.2 mGy cm).

Image reconstruction and post-processing

Each DECT scan can obtain three types of images: 80-kVp, Sn140-kVp, and weighted average images. The weighted average image, calculated at a ratio of 0.3:0.7 based on the data of tube A and tube B, is similar to the standard CT image, which possess the contrast characteristic of a 120-kVp. To the postprocessing data of DECT, 0.6 mm thickness axial sections were reconstructed from the 80- and Sn140-kVp datasets. The CT images were postprocessed with software (Syngo, MMWP VE40B; Siemens Healthineers). Set the relative contrast ratio to 1.56 at 80- and Sn140 kVp. The strength of the smoothing filter was set to 4. For further analysis, VNCa images were displayed on grey-scale and color-coded maps.

MRI acquisition

A 3.0T imaging system (Achieva; Philips Healthcare) with a phased-array knee coil was used to conduct all MRI examinations. We have collected the following sequences: Axial Spectral Attenuated Inversion Recovery sequence (SPAIR), Sagittal SPAIR sequence, coronal SPAIR sequence, and Sagittal T1-weighted Turbo Spin Echo sequence, with specific parameters as shown in Table S2. The interested reader can find them in a supplementary appendix online.

Qualitative analysis

BMLs were scored in each subregion of per knee. Each knee joint was divided into a total of 15 subregions. The patella and tibial plateau were divided into medial and lateral. The medial patella including patellar ridge. Subspinous region was listed as a separate part. As for the articular surface of the femur, it was divided into medial (including trochlear groove) and lateral condyles. Simultaneously the medial/lateral tibial plateau and femur condyle were further divided into three subregions: anterior, central and posterior[35].

BML scores in DECT images were analyzed by reader 1 (H.L.) and reader 2 (W.C.) independently, 6 and 4 years of experience in musculoskeletal radiology, respectively. They were unaware of clinical information and MRI results. BMLs no less than 2 mm away from the cortical bone was included for further analysis. As a result of the extent of BMLs in the affected area, the following severity score was assigned: subregions without BMLs were classified as Grade 1 (0 score); suspected or mild BMLs with a diameter less than 5 mm were classified as Grade 2 (1 score); moderate BMLs with a diameter 5 mm to 2 cm were classified as Grade 3 (2 score); severe BMLs with a diameter > 2 cm were classified as Grade 4 (3 score)[36]. Grade 1–4 BMLs on MRI and DECT VNCa images were shown in Fig. 2. By summing the BML score of 15 subregions, the total BML scores of the knee joint (range 0–45) was obtained. The higher the total BML score of the knee, the more severe degree of BMLs.

Meanwhile, the MRI was utilized as the reference standard. BMLs were graded using the CT scoring system previously mentioned. A third reader (F.P., who has 10 years of experience in musculoskeletal imaging) evaluated MR images for the presence of BMLs. Results of DECT was not disclosed to Reader 3.

Quantitative analysis

The readers 1 and 2 independently analyzed the quantitative images after the qualitative images were analyzed. A circular region of interest (ROI) was manually placed in the area with the highest BML intensity on VNCa images to determine CT numbers. However, ROI is placed in the center of the subregion in areas without bone marrow lesions.

Statistical analysis

Cohen's kappa (κ) statistics was used to evaluate the inter-reader agreement in qualitative analysis of dual-energy VNCa images. CT numbers were compared between different grades of BMLs by using the Kruskal-Wallis test. In order to evaluate CT numbers derived from VNCa images, the receiver operating characteristic curve (ROC) was analyzed and the area under the ROC curve (AUC) calculated. Following that, ROC analysis was used to compare average CT numbers with MR images to determine the CT number that showed the highest accuracy for detecting BMLs. Sensitivity and specificity were calculated based on this cutoff value. Correlation analysis between total BML scores on DECT/MRI and two pain scales based on Spearman's correlation coefficient.

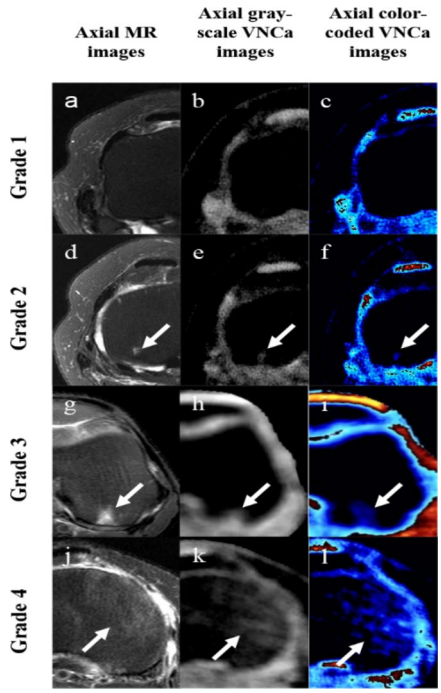

Fig. 2. A series of axial spectral attenuated inversion recovery MRI images, gray-scale virtual noncalcium (VNCa) images, and corresponding color-coded mapping images for Grade 1–4 bone marrow lesions (BMLs). (**a–c**) Present axial MRI, gray-scale VNCa, and color-coded mapping images depicting Grade 1 BMLs in the tibial. (**d–f**) Present axial MRI, gray-scale VNCa, and color-coded mapping images depicting Grade 2 BMLs in the tibial. (**g–i**) present axial MRI, gray-scale VNCa, and color-coded mapping images depicting Grade 3 BMLs in the condyles of femur. (**j–l**) present axial MRI, gray-scale VNCa, and color-coded mapping images depicting Grade 4 BMLs in the tibia.

Parameter	Value
Mean age ± SD, range (years)	58.87 ± 7.41, 43–76
Sex	
Men	7 (30.43%)†
Women	16 (69.57%)†
The extent of BMLs on MRI	
Grade 1	308(76.05%)†
Grade 2	50 (12.35%)†
Grade 3	16 (3.95%)†
Grade 4	31 (7.65%)†
Pain assessment	
Mean WOMAC ± SD, range	22.59 ± 7.72 (10–42)
Mean KOOS ± SD, range	0.76 ± 0.14 (0.35–0.91)

Table 1. Characteristics of participants in this study. *SD* = standard deviation, *BMLs* = bone morrow lesions, *MRI* = magnetic resonance imaging, *WOMAC* = the Western Ontario and McMaster Universities Osteoarthritis Index, *KOOS* = the Knee Injury and Osteoarthritis Outcome Score. †Data are numbers of cases, with percentages in parentheses.

Using SPSS 25.0 and MedCalc software to analyze data, and make 0.05 the boundary of statistical significance. Continuous variables were expressed as mean ± standard deviations (M ± SD).

Results

Study participants

Twenty-three patients were screened (mean age, 58.87 ± 7.41 years; age range, 43–76 years), including 16 women (mean age, 59.06 ± 7.87 years; age range, 43–76 years) and 7 men (mean age, 59.57 ± 6.78 years; age range, 47–66 years). The Table 1 shows the demographics and characteristics of the participants.

Parameter	Reader 1	Reader 2
Sensitivity (%)	89.4 (76.1, 96.0)	87.2 (73.6, 94.7)
Specificity (%)	99.4 (97.8, 99.9)	99.2 (97.4, 99.8)
PPV (%)	95.5 (83.3, 99.2)	93.2 (80.3, 98.2)
NPV (%)	98.6 (96.6, 99.5)	98.3 (96.2, 99.3)

Table 2. Visual image analysis of bone marrow lesions in knee osteoarthritis patients on dual-energy CT for two readers. Data are percentages, with 95% confidence intervals in parentheses. *PPV* = positive predictive value, *NPV* = negative predictive value.

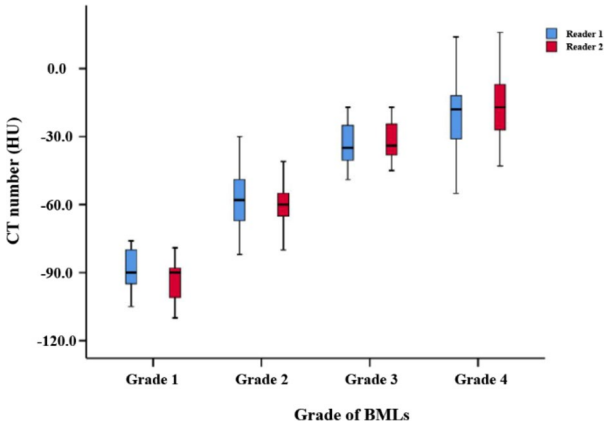

Fig. 3. Box-and-whisker plots show mean dual-energy CT numbers (in Hounsfield units) measured on virtual noncalcium images for all cases. Boundaries of boxes indicate lower and upper quartiles, and lines in boxes indicate medians.

A total of 405 subregions were analyzed, of which 97 subregions showed BMLs on MRI. According to the extent of BMLs in the knee joint, MRI classified 308 subregions as Grade 1, 50 as Grade 2, 16 as Grade 3, and 31 as Grade 4. The mean pain score of WOMAC and KOOS was 22.59 and 0.76, respectively (Table 1).

Qualitative analysis

Inter-reader agreement of VNCa images assessment was excellent for two readers ($\kappa = 0.91$). When MRI at grade 3–4 was counted as positive for BMLs and grade 1–2 was counted as negative. For reader 1, two subregions that had no BMLs on MRI were identified as having BMLs on VNCa images, the result classification was false positive. five of which were classified as being BML-free on VNCa images were found to have BMLs on MRI, these findings were classified as false-negatives. For reader 2, a total of three false positives and six false negatives of BMLs were detected in images from VNCa. For diagnosis of BMLs with VNCa images, reader 1 achieved overall sensitivity of 89.4% (95%CI: 76.1, 96.0%), specificity of 99.4% (95%CI: 97.8, 99.9%), positive predictive value (PPV) of 95.5% (95%CI: 83.3, 99.2%) and negative predictive value (NPV) of 98.6% (95%CI: 96.6, 99.5%). For reader 2, the corresponding values were 87.2% (95%CI: 73.6, 94.7%), 99.2% (95%CI: 97.4, 99.8%), 93.2% (95%CI: 80.3, 98.2%), and 98.3% (95%CI: 96.2, 99.3%) (Table 2).

Quantitative analysis

Mean CT numbers corresponding to different grade BMLs on VNCa images of reader 1 and reader 2 were shown in Table S3. There was statistical significance between the mean CT numbers of different grade BMLs on VNCa images ($P < 0.001$ for both readers). The CT numbers of BMLs increased with the BML grade (Fig. 3).

Table S4 showed the CT numbers of positive and negative oedema areas according to MRI. For reader 1, the AUC for separating positive from negative oedema areas were 0.970 (95% CI: 0.919, 0.993). While for reader 2, it was 0.996 (95% CI: 0.958, 1.00) (Fig. 4, $P < 0.001$ for both readers). According to reader 1, the cutoff value of − 41.5 HU yielded a sensitivity of 93.2% (95%CI:81.3, 98.6%) and specificity of 90.9% (95%CI: 81.3, 96.6%), and it was − 46.5 HU for reader 2 that achieved a sensitivity of 100.0% (95%CI: 92.0, 100.0%) and specificity of 93.9% (95%CI: 85.2, 98.3%) (Table 3).

Correlation between total BML scores and pain scale assessment

The pain scores on WOMAC were strong positive correlation to total BML scores on DECT ($r = 0.774$, 0.723, respectively, $P < 0.001$) and MRI ($r = 0.802$, $P < 0.001$) (Fig. 5a–c). In contrast, the pain scores on KOOS were highly negatively related to the total BML scores on DECT (− 0.695, − 0.789, respectively, $P < 0.001$) and MRI ($r = -0.680$, $P < 0.001$) (Fig. 5d–f). In short, the degree of knee pain increased with the severity of BMLs.

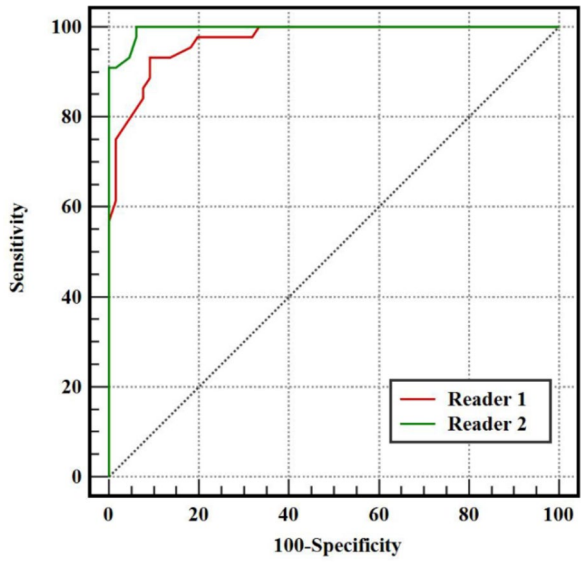

Fig. 4. Receiver operating characteristic (ROC) curves calculated from CT numbers (HU) derived from dual-energy virtual noncalcium (VNCa) images of two readers. Area under the receiver operating characteristics curve was 0.970 for reader 1 and 0.996 for reader 2.

Parameters	Reader 1	Reader 2
Sensitivity (%)	93.2 (81.3, 98.6)	100.0 (92.0, 100.0)
Specificity (%)	90.9 (81.3, 96.6)	93.9 (85.2, 98.3)
Area under the ROC curve	0.970 (0.919, 0.993)	0.996 (0.958, 1.000)
Cutoff CT value (HU)	− 41.5	− 46.5

Table 3. Diagnostic performance of dual-energy virtual non-calcium technique in quantitative analysis of region of interest–based mean attenuation measurement. Data are percentages, with 95% confidence intervals in parentheses. *ROC* = receiver operating characteristic.

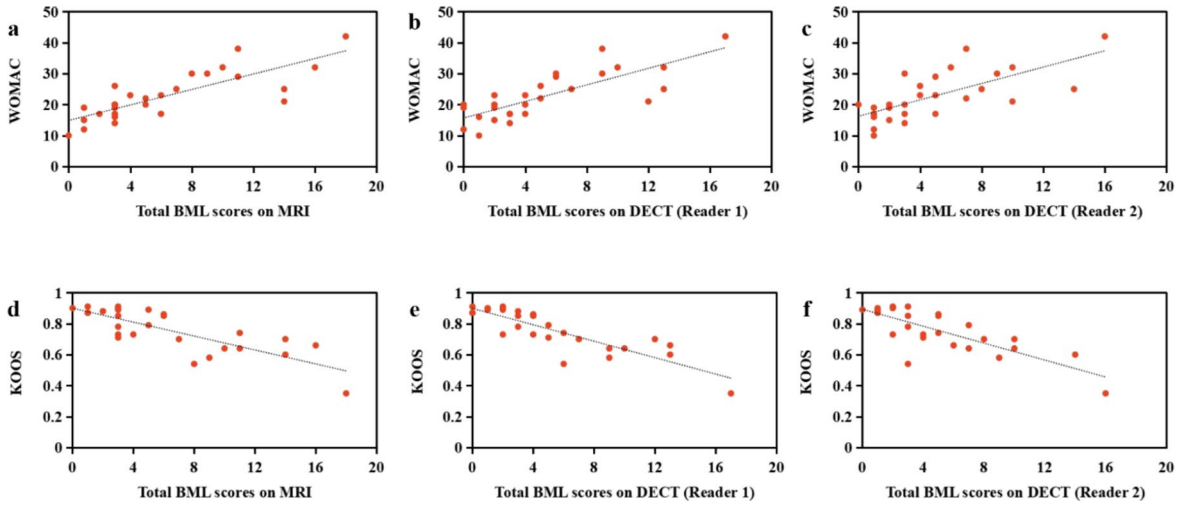

Fig. 5. Correlation between the clinical pain scores and bone marrow lesions (BMLs). (**a–c**) positive correlation between the Western Ontario and McMaster Universities Osteoarthritis Index (WOMAC) and total BML scores on MRI and dual-energy computed tomography (DECT) ($r = 0.802$, 0.774, 0.723, *respectively*, $P < 0.001$), (**d–f**) negative correlation between the Knee Injury and Osteoarthritis Outcome Score (KOOS) and total BML scores on MRI and DECT ($r = -0.680$, − 0.695, − 0.789, respectively, $P < 0.001$).

Discussion

Taking MRI as the standard of reference, we used DECT VNCa technique to analyze the relationship between pain scale and BML score in knee OA patients. As a result of our primary findings, we concluded that DECT was capable of detecting BMLs with an excellent AUC, high specificity, and PPV. Meanwhile, the CT numbers of BMLs increased with the BML grade. Furthermore, we found a strong correlation between BML score and pain scale in knee OA patients.

This study only included BMLs located 2 mm away from adjacent cortical bone, with the aim of minimizing artifacts that interfere with the accuracy of BML assessment. In our qualitative analysis, the visualization of BMLs by DECT images and VNCa applications showed good diagnostic performance, which corresponded well to those of previous studies in non-traumatic settings[12,22–24,37]. Especially in the study conducted by Foti et al.[24], focused on osteochondral lesions of the ankle, the sensitivity and specificity of BMLs around the ankle joint in non-traumatic patients reached 89.7% and 81.8% respectively. In another study, DECT was found to depict the bone marrow changes surrounding stress fractures caused by repeated microtrauma over time. High-resolution morphological CT images clearly demonstrate the course of a fracture line, and differentiate between fresh fractures and old fractures based on the presence of reactive osteoblastic response[22]. Also, this is similar to the results of VNCa studies of various joint trauma reported previously, such as knee[11], wrist[38], vertebral bodies[17] and hip[39]. Although DECT has limited capability in assessing soft tissue injuries, such as meniscal or ligamentous damage, it serves as an alternative or supplementary imaging method for MRI in detecting BMLs, especially when patients have contraindications for MRI or in the case of emergency[18]. Additionally, CT scans are less expensive and time consumption than MRI.

According to VNCa, we discovered that CT numbers of BMLs in positive areas were significantly higher than that in negative areas. Besides, based on ROC analysis, the sensitivity and specificity for distinguishing BMLs from non-BMLs of the knee joint were 93.2% and 90.9% for reader 1, 100.0% and 93.9% for reader 2, respectively. This is similar to previous findings based on ROI-based mean attenuation measurement in distinguishing BMLs from non-BMLs in ankle and sacroiliac joint[12,15]. Therefore, the difference in CT numbers between BMLs positive and negative areas is the main factor affecting the diagnosis of VNCa images, which enables BMLs to be discovered in VNCa images and further demonstrates the value of DECT in diagnosing BMLs in OA patients. In addition to the application of VNCa technique, different types of VNCa images, such as color-coded images, can also be used to help better detect bone marrow attenuation changes and improve the performance of VNCa images in displaying abnormal bone marrow.

We found the dual-energy VNCa CT numbers gradually increased with the BML grade between both readers. Meanwhile, calculations have shown a statistically significance difference between different BML grade in CT numbers, which is in good agreement with considerable BML CT-number studies that have been reported on VNCa images[12,40,41]. There are similarities and differences in the pathologic basis of increased CT numbers of BMLs according to the etiology. For example, pathological manifestations of BMLs caused by arthritis induces increased fluid content and decreased fat content[42]. Alternatively, trabecular microfractures, oedema, and hemorrhage after acute trauma can cause increased amounts of interstitial fluid and blood, thereby increasing the CT number[11,13]. Thus, we consider that the reason of OA-BMLs CT-number increasing is similar to that mentioned above, which may be the increase of fluid.

In our study, the optimal cutoff value for diagnosing BMLs on VNCa was − 41.5 HU and − 46.5 HU, which is highly similar to the results of patient with sacroiliitis that reported by Wu et al. (− 33.4 HU and − 42.35 HU)[12] and Chen M et al. (− 40.8 HU and − 44.4 HU)[19], and Zuo et al. in the osteonecrosis of the femoral head (− 57.2 HU)[37]. The slight discrepancies of the cutoff value in these observations of non-traumatic joints could be explained by different ages, anatomic structures, the usage of divers CT scanners, differing kilovoltage settings, and postprocessing algorithms[11,17,43]. Unsurprisingly, many studies revealed higher cut-off values for traumatic BMLs in the vertebra (− 0.43 HU, − 11.8 HU)[17,44], wrist (5.90 HU)[45], and knee (1.45 HU)[46], which is mainly due to the histological changes of hemorrhage and hyperemia after trauma, especially hemorrhage[47].

Our study showed that the knee pain degree increased with the severity of BMLs depicted on DECT and MRI. This is in accordance with various studies that BMLs were positively correlated with the severity of knee pain[8–10]. Nevertheless, some studies failed to find an association between BMLs and pain severity[48,49]. The reasons for discrepancies in findings regarding the association between BMLs and pain severity may be as follows. First, a difference in clinical symptoms may be related to the different pathological changes with BMLs. For example, oedema and microfractures are highly reminiscent to pain, while fibrotic changes would be rather painless[48]. Second, as a result of different MR pulse sequences, different presentation of BMLs will be produced. Generally, BMLs measured on 3D dual echo steady state sequences will underestimate BML size and change, weaken the correlation between BMLs and pain severity[49]. Based on the excellent diagnostic performance of VNCa for BMLs and the strong correlation between BMLs and pain severity in this study, we believe that DECT will play an essential role in the pain assessment of patients with knee osteoarthritis for years to come, especially those who are contraindicated or not applicable to MRI.

Interestingly, overall, the WOMAC had a stronger correlation with total BMLs score compared with KOOS. This may be due to the fact that our study participants were mainly elderly. Currently, WOMAC is the main scale used to clinically evaluate pain in senile degenerative bone and joint diseases[34]. KOOS, an extension of WOMAC, is developed for younger and/or more active patients with knee injury and/or knee osteoarthritis[50]. To a certain extent, this study also demonstrated that different pain assessment scale had differing applicable populations.

Lastly, we would like to briefly discuss the evolution of CT technology. Until recently, energy-integrating detector CT (EID-CT) represented the stronghold hardware technology of CT data acquisition. With the approval of photon-counting CT (PCD-CT) for clinical use in 2021, represents the most recent innovation in CT technology. In terms of CT detector technology, PCD-CT employs semiconductor detectors that can directly

convert X-ray photons into electrical signals[51,52], eliminating the need for the photoelectric conversion step required by EID-CT[52–54]. This innovation not only eradicates electronic (background) noise but also enhances the efficiency of X-ray photon utilization and strengthens the intensity of iodine signals. The smaller photon detector elements of PCD-CT significantly improve spatial resolution[55,56]. Additionally, by eliminating the septa, which were traditionally employed to prevent fluorescence cross-talk in the detector, the radiation dose is reduced[52,56,57]. Unlike EID-CT, which measures photon energy as an integrated sum of detected energies, PCD-CT counts individual x-ray photons and their respective energies with equal weight, realizing genuine multi-spectral imaging[54]. This makes CT examinations more accurate and safer, expanding the clinical applications of CT.

There are several limitations to this study. First, our study sample was small. Second, owing to the limitation of VNCa algorithm, mild BMLs directly adjacent to cortical bone can't be displayed. Therefore, mild BMLs next to cortical bone are prone to loss by reason of incomplete masking of the cortex as well as spatial averaging[12].

In conclusion, the VNCa dual-energy images are capable of detecting BMLs in knee OA both qualitatively and quantitatively. Furthermore, the pain degree increased with the severity of BMLs on VNCa images, DECT has the potential to predict pain by grading BMLs, thereby provide help for clinical diagnosis and treatment of knee OA patients.

Data availability

The original contributions presented in the study are included in the article/Supplementary Material. Further inquiries can be directed to the corresponding authors.

Received: 21 August 2024; Accepted: 13 January 2025
Published online: 27 January 2025

References

1. Gardashli, M. et al. The roles of regulatory-compliant media and inflammatory/oxytocin priming selection in enhancing human mesenchymal stem/stromal cell immunomodulatory properties. *Sci. Rep.* **14** (1), 29438 (2024).
2. Barr, A. J. et al. A systematic review of the relationship between subchondral bone features, pain and structural pathology in peripheral joint osteoarthritis. *Arthritis Res. Ther.* **17** (1), 228 (2015).
3. Satake, Y., Izumi, M., Aso, K. & Ikeuchi, M. Association between infrapatellar fat pad ultrasound elasticity and anterior knee pain in patients with knee osteoarthritis. *Sci. Rep.* **13** (1), 20103 (2023).
4. Alliston, T., Hernandez, C. J., Findlay, D. M., Felson, D. T. & Kennedy, O. D. Bone marrow lesions in osteoarthritis: what lies beneath. *J. Orthop. Res.* **36** (7), 1818–1825 (2018).
5. Ge, L., Zhang, X., Zhu, R. & Cai, G. Bone marrow lesions in osteoarthritis: biomarker or treatment target? A narrative review. *Skelet. Radiol.* **54** (2), 175–191 (2025).
6. Sofat, N. & Howe, F. A. Bone marrow lesions in osteoarthritis: characterising genetic and histological changes to understand disease pathophysiology. *Osteoarthr. Cartil. Open* **6** (4), 100531 (2024).
7. Aso, K., Sugimura, N., Wada, H., Deguchi, S. & Ikeuchi, M. Increased nerve growth factor expression and osteoclast density are associated with subchondral bone marrow lesions in osteoarthritic knees. *Osteoarthr. Cartil. Open* **6** (3), 100504 (2024).
8. Aso, K., Shahtaheri, S. M., McWilliams, D. F. & Walsh, D. A. Association of subchondral bone marrow lesion localization with weight-bearing pain in people with knee osteoarthritis: Data from the osteoarthritis initiative. *Arthritis Res. Ther.* **23** (1), 35 (2021).
9. Chua, K. et al. Subchondroplasty for bone marrow lesions in the arthritic knee results in pain relief and improvement in function. *J. Knee Surg.* **34** (6), 665–671 (2021).
10. Wang, X. et al. Synovitis mediates the association between bone marrow lesions and knee pain in osteoarthritis: data from the Foundation for the National Institute of Health (FNIH) osteoarthritis biomarkers Consortium. *Osteoarthr. Cartil.* **30** (9), 1270–1277 (2022).
11. Booz, C. et al. Color-coded virtual non-calcium dual-energy CT for the depiction of bone marrow edema in patients with acute knee trauma: A multireader diagnostic accuracy study. *Eur. Radiol.* **30** (1), 141–150 (2020).
12. Wu, H. et al. Axial spondyloarthritis: dual-energy virtual noncalcium CT in the detection of bone marrow edema in the sacroiliac joints. *Radiology* **290** (1), 157–164 (2019).
13. Ren, Q., Tang, D., Xiong, Z., Zhao, H. & Zhang, S. Traumatic bone marrow lesions in dual-energy computed tomography. *Insights Imaging* **13** (1), 174 (2022).
14. Guggenberger, R. et al. Diagnostic performance of dual-energy CT for the detection of traumatic bone marrow lesions in the ankle: comparison with MR imaging. *Radiology* **264** (1), 164–173 (2012).
15. Foti, G. et al. Identification of bone marrow edema of the knee: diagnostic accuracy of dual-energy CT in comparison with MRI. *Radiol. Med.* **126** (3), 405–413 (2021).
16. Ghazi Sherbaf, F. et al. DECT in detection of vertebral fracture-associated bone marrow edema: a systematic review and meta-analysis with emphasis on technical and imaging interpretation parameters. *Radiology* **300** (1), 110–119 (2021).
17. Cavallaro, M. et al. Comprehensive comparison of dual-energy computed tomography and magnetic resonance imaging for the assessment of bone marrow edema and fracture lines in acute vertebral fractures. *Eur. Radiol.* **32** (1), 561–571 (2022).
18. Ahmad, M. I., Liu, L., Sheikh, A. & Nicolaou, S. Dual-energy CT: Impact of detecting bone marrow oedema in occult trauma in the emergency. *BJR Open* **6** (1), tzae025 (2024).
19. Chen, M. et al. Bone marrow edema in sacroiliitis: detection with dual-energy CT. *Eur. Radiol.* **30** (6), 3393–3400 (2020).
20. Fervers, P. et al. Feasibility of artificial intelligence-supported assessment of bone marrow infiltration using dual-energy computed tomography in patients with evidence of monoclonal protein—A retrospective observational study. *Eur. Radiol.* **32** (5), 2901–2911 (2022).
21. Tan, M. T. & Lloyd, T. B. Utility of dual energy computed tomography in the evaluation of infiltrative skeletal lesions and metastasis: a literature review. *Skelet. Radiol.* **51** (9), 1731–1741 (2022).
22. Foti, G. et al. Identification of non-traumatic bone marrow oedema: the pearls and pitfalls of dual-energy CT (DECT). *Tomography* **7** (3), 387–396 (2021).
23. Foti, G. et al. Bone marrow edema around the hip in non-traumatic pain: dual-energy CT vs MRI. *Eur. Radiol.* **30** (7), 4098–4106 (2020).
24. Foti, G. et al. Identification of bone marrow edema around the ankle joint in non-traumatic patients: diagnostic accuracy of dual-energy computed tomography. *Clin. Imaging* **69**, 341–348 (2021).
25. Bouman, C. M. B. et al. Assessment of bone marrow edema on dual-energy CT scans in people with diabetes mellitus and suspected Charcot neuro-osteoarthropathy. *Skelet. Radiol.* **54** (1), 105–112 (2025).

26. Xu, G. et al. Diagnostic value of dual-energy CT virtual noncalcium for the assessment of bone marrow edema of wrist in patients with rheumatoid arthritis. *Acad. Radiol.* **31** (9), 3740–3748 (2024).
27. Alizai, H. et al. Cartilage lesion score: comparison of a quantitative assessment score with established semiquantitative MR scoring systems. *Radiology* **271** (2), 479–487 (2014).
28. Hayashi, D., Roemer, F. W. & Guermazi, A. Imaging for osteoarthritis. *Ann. Phys. Rehabil. Med.* **59** (3), 161–169 (2016).
29. Wang, Y. et al. Meniscal extrusion predicts increases in subchondral bone marrow lesions and bone cysts and expansion of subchondral bone in osteoarthritic knees. *Rheumatology* **49** (5), 997–1004 (2010).
30. Roi, G. S., Monticone, M., Salvoni, M., Sassi, R. & Alberti, G. Self-reported knee symptoms assessed by KOOS questionnaire in downhill runners (Skyrunners). *PLoS ONE* **10** (4), e0126382 (2015).
31. Cronström, A., Creaby, M. W., Nae, J. & Ageberg, E. Modifiable factors associated with knee abduction during weight-bearing activities: a systematic review and meta-analysis. *Sports Med.* **46** (11), 1647–1662 (2016).
32. Carek, S. M. Hip and knee injuries. *Prim. Care* **47** (1), 115–131 (2020).
33. Freystaetter, G. et al. Total serum testosterone and western Ontario and McMaster universities osteoarthritis Index pain and function among older men and women with severe knee osteoarthritis. *Arthritis Care Res. (Hoboken)* **72** (11), 1511–1518 (2020).
34. Roos, E. M. & Toksvig-Larsen, S. Knee injury and osteoarthritis outcome score (KOOS)—Validation and comparison to the WOMAC in total knee replacement. *Health Qual. Life Outcomes* **1**, 17 (2003).
35. Peterfy, C. G. et al. Whole-organ magnetic resonance imaging score (WORMS) of the knee in osteoarthritis. *Osteoarthr. Cartil.* **12** (3), 177–190 (2004).
36. Vishavpreet, S., Ali, O., Timothy, T., Azzam, F. & Alisina, S. Clinical and pathophysiologic significance of MRI identified bone marrow lesions associated with knee osteoarthritis. *Arch. Bone Jt. Surg.* **7** (3), 211–219 (2019).
37. Zuo, T. et al. Detection of bone marrow edema in osteonecrosis of the femoral head using virtual noncalcium dual-energy computed tomography. *Eur. J. Radiol.* **139**, 109681 (2021).
38. Koch, V. et al. Incremental diagnostic value of color-coded virtual non-calcium dual-energy CT for the assessment of traumatic bone marrow edema of the scaphoid. *Eur. Radiol.* **31** (7), 4428–4437 (2021).
39. Kellock, T. T. et al. Detection of bone marrow edema in nondisplaced hip fractures: utility of a virtual noncalcium dual-energy CT application. *Radiology* **284** (3), 798–805 (2017).
40. Poort, L. J. et al. Detection of bone marrow edema pattern with dual-energy computed tomography of the pig mandible treated with radiotherapy and surgery compared with magnetic resonance imaging. *J. Comput. Assist. Tomogr.* **41** (4), 553–558 (2017).
41. Cao, J. X., Wang, Y. M., Kong, X. Q., Yang, C. & Wang, P. Good interrater reliability of a new grading system in detecting traumatic bone marrow lesions in the knee by dual energy CT virtual non-calcium images. *Eur. J. Radiol.* **84** (6), 1109–1115 (2015).
42. Zanetti, M., Bruder, E., Romero, J. & Hodler, J. Bone marrow edema pattern in osteoarthritic knees: correlation between MR imaging and histologic findings. *Radiology* **215** (3), 835–840 (2000).
43. Wellenberg, R. H. H. et al. Quantitative evaluation of the effects of dual-energy CT acquisition, reconstruction and postprocessing parameters on virtual non-calcium (VNCa) images. *Eur. J. Radiol.* **182**, 111818 (2025).
44. Wang, Y. et al. Detection of different degree traumatic vertebral bone marrow oedema by virtual non-calcium technique of dual-source dual-energy CT. *Clin. Radiol.* **75** (2), e11–e19 (2020).
45. Ali, I. T. et al. Clinical utility of dual-energy CT analysis of bone marrow edema in acute wrist fractures. *Am. J. Roentgenol.* **210** (4), 842–847 (2018).
46. Liang, J., Fang, Y., Jiang, Y., Zhan, Y. & Hong, G. Diagnostic accuracy of dual-energy CT virtual non-calcium images with different related contrast material values for the detection of bone marrow edema in knee. *Eur. J. Radiol.* **133**, 109385 (2020).
47. Eriksen, E. F. & Ringe, J. D. Bone marrow lesions: a universal bone response to injury? *Rheumatol. Int.* **32** (3), 575–584 (2012).
48. Cai, G. et al. The association between change in bone marrow lesion size and change in tibiofemoral cartilage volume and knee symptoms. *Rheumatology* **60** (6), 2791–2800 (2021).
49. Zhang, M., Driban, J. B., Price, L. L., Lo, G. H. & McAlindon, T. E. Magnetic resonance image sequence influences the relationship between bone marrow lesions volume and pain: Data from the osteoarthritis initiative. *Biomed. Res. Int.* **2015**, 731903 (2015).
50. Roos, E. M., Roos, H. P., Lohmander, L. S., Ekdahl, C. & Beynnon, B. D. Knee injury and osteoarthritis outcome score (KOOS)—Development of a self-administered outcome measure. *J. Orthop. Sports Phys. Ther.* **28** (2), 88–96 (1998).
51. Carrino, J. A. et al. CT in musculoskeletal imaging: still helpful and for what? *Skelet. Radiol.* **53** (9), 1711–1725 (2024).
52. Toia, G. V. et al. Approaches, advantages, and challenges to photon counting detector and multi-energy CT. *Abdom. Radiol.* **49** (9), 3251–3260 (2024).
53. Mourad, C. et al. Chances and challenges of photon-counting CT in musculoskeletal imaging. *Skelet. Radiol.* **53** (9), 1889–1902 (2024).
54. Baffour, F. I. et al. Photon-counting detector CT for musculoskeletal imaging: a clinical perspective. *Am. J. Roentgenol.* **220** (4), 551–560 (2023).
55. Demehri, S. et al. Musculoskeletal CT imaging: state-of-the-art advancements and future directions. *Radiology* **308** (2), e230344 (2023).
56. Heismann, B., Kreisler, B. & Fasbender, R. Photon counting CT versus energy-integrating CT: A comparative evaluation of advances in image resolution, noise, and dose efficiency. *Med. Phys.* **1**, 1 (2024).
57. Rajendran, K. et al. Improved visualization of the wrist at lower radiation dose with photon-counting-detector CT. *Skelet. Radiol.* **52** (1), 23–29 (2023).

Acknowledgements

This study has received funding by the Scientific Research Project of Hunan Provincial Department of Education, Key project (Grant No. 20A437 (H. Z.)), Hunan Provincial Science and Technology Innovation Program of China (Grant No. 2017SK50203 (H. Z.)), the Natural Science Foundation of Hunan Province of China (Grant No. 2021JJ30621 (D.T.)), and the Scientific Research Project of Hunan Provincial Health Commission (Grant Nos. 202109010099 (D.T.), 202109040556 (H.L.), 202209014251 (X.C.), D202309019457 (H.L.)).

Author contributions

Author Contributions(I) Conception and design: Heng Zhao, Limin Liu(II) Administrative support: De-qiu Tang, Heng Zhao(III) Provision of study materials or patients: Fei Peng, Wei Chen, Hui Li(IV) Collection and assembly of data: Jing Luo, Yao-lin Qu, Dan Zhang, Ya-han He, Yi-sha Pan, Fang Gao, (V) Data analysis and interpretation: Hua-zhi Liao, Xiao-long Chen, Hao Lei, (VI) Manuscript writing: All authors(VII) Final approval of manuscript: All authors.

Declarations

Competing interests
The authors declare no competing interests.

Ethical approval
The studies involving human participants were reviewed and approved by the Institutional Review Board of the First Affiliated Hospital of University of South China. And informed consents were obtained from all participants before examination. It was also registered in China Clinical Trial Registry Center (Registration number: ChiCTR1900024305).

Additional information
Supplementary Information The online version contains supplementary material available at https://doi.org/10.1038/s41598-025-86697-2.

Correspondence and requests for materials should be addressed to F.P.

Reprints and permissions information is available at www.nature.com/reprints.

Publisher's note Springer Nature remains neutral with regard to jurisdictional claims in published maps and institutional affiliations.